

Rational Design of Highly Responsive pH Sensors Based on DNA i-Motif

Irina V. Nesterova* and Evgueni E. Nesterov

Table of Contents

Experimental Methods	page S1
DNA i-motif: Structure and Properties	page S3
Table S1	page S4
Table S2	page S5
Figures S1 and S2	page S10
Figure S3	page S11
Figure S4	page S12
Figure S5	page S13
Figure S6	page S14
Figure S7	page S15
Figure S8	page S16
Figure S9	page S17
References	page S18

Experimental Methods

Reagents and Materials. All the chemical reagents were obtained from established commercial suppliers (i.e. Sigma-Aldrich (St. Louis, MO), Fisher Scientific (Pittsburg, PA) and others). Nuclease-free water used for preparation of DNA solutions was obtained from IDT (Coralville, IA). Phosphate buffers (Na_2HPO_4 (20 mM)/KCl (100 mM)) were prepared in house. Single stranded DNAs (including fluorophore/quencher labeled) were obtained from IDT (Coralville, IA) and reconstituted with nuclease-free water. pH-meter calibration buffers (4.00 ± 0.01 , 7.00 ± 0.01 , and 10.00 ± 0.02) were purchased from Fisher. Fetal Bovine Serum (FBS) was obtained from Sigma.

Preparation of buffers. A stock buffer solution consisting of Na_2HPO_4 (20 mM)/KCl (100 mM) was prepared and split into approx. 20 mL aliquots. pH of every aliquot was adjusted to an appropriate value using H_3PO_4 and/or NaOH immediately after pH-meter calibration/accuracy check. pH of each buffer aliquot was verified every time when samples were prepared using a calibrated pH meter. Actual pH values were utilized in all reported calculations.

Measuring pH. ThermoOrion pH-meter (model 420) was used throughout the studies. The pH meter was calibrated every time it was used against fresh aliquots of pH calibration buffers. The pH meter accuracy was confirmed over the calibration range against pH calibration buffers and never exceeded buffers' nominal value ± 0.02 units.

Sample preparation for pH denaturation studies. A typical sample (500 μL) was prepared by diluting an oligonucleotide stock solution (to concentration of 0.5-1 μM for UV studies and 0.1 μM for fluorescent studies) with an appropriate buffer, heating the solution at 95°C for 10 minutes followed by slow (overnight) cooling to room temperature. The monomolecularity of an i-motif folding has been established (for similar conditions) for concentrations below 10 μM .¹ Therefore, we can assume that all the denaturations studied involved intramolecularly folded structures.

pH Denaturation studies by UV. pH Denaturation studies via UV spectroscopy were performed using a Cary 5000 UV-Vis-NIR spectrophotometer (Agilent Technologies, Santa Clara, CA). Typically, measurements were performed on a 500- μL aliquot of a 0.5-1.0 μM sample using a 10 mm optical path cuvette. The i-motif transformations were monitored at 295 nm where C-quadruplex unfolding is accompanied by the hypochromic effect.² The measurements were taken at room temperature and corrected against corresponding blank buffers. An example of absorption changes upon pH-triggered denaturation of an oligonucleotide is included in Figure S9.

pH Denaturation studies by fluorescence. pH-Dependent denaturation studies via fluorescence were carried out using a QuantaMaster4/2006SE spectrofluorimeter (PTI, Birmingham, NJ). Typically, the measurements were performed on a 100 μL aliquot of a 100 nM sample. Fluorescence of Rhodamine Green was excited at the wavelength of 495 nm with emission spectra typically recorded between 510 and 630 nm. Maximum emission (531 nm) was used for plotting denaturation profiles.

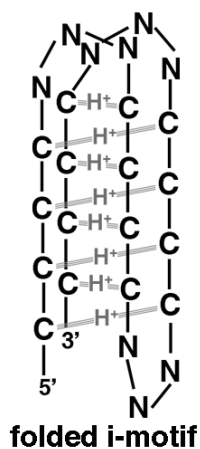
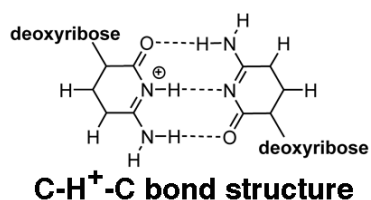
For studies in the presence of serum, the sensors were prepared in phosphate buffers as described above. After addition of appropriate amount of FBS (to yield 20 %), the samples were equilibrated with serum for 1 hour before the emission measurements were taken. pH of buffer/serum (80/20) mixtures were determined since serum possesses buffering capacity and therefore may shift buffer pH. Actual buffer/serum mixtures pH values were utilized to plot pH-denaturation profiles.

Data processing. The values reported throughout the Communication (i.e. pH^T , ΔpH_{10-90} , and n) were derived from pH denaturation curves. Average values derived from at least 2-3 separate pH-denaturation profiles were determined for each parameter (Table S2).

In order to determine pH^T and ΔpH_{10-90} , the *signal* (UV at 295 nm or fluorescence at 531 nm) vs. *pH* data points were plotted and fitted with Boltzmann sigmoidal fits using Origin 8.5.1 software. The values for “ x_0 ” (point of inflection) were reported as pH^T 's. The widths of pH intervals corresponding to signal changing from 10 to 90 % were reported as ΔpH_{10-90} 's.

In order to determine n , the *signal* (i.e. UV at 295 nm) vs. H^+ -*concentration* data points were plotted and fitted with a two-state Hill equation using Origin 8.5.1 software. The values for “ n ” were reported as Hill coefficients.

DNA i-motif: structure and properties



Scheme S1.

type), and/or interference from As due to their increased affinity towards proton binding,⁶ and/or other reasons (e.g. base stacking interactions well established for hairpin loops⁷ but not yet studied for i-motifs).

The thermodynamic stability of hemiprotonated Cytidine-H⁺-Cytidine base pairs (in acidic media) is comparable with the stability of the classic Watson-Crick base pairs. *Per base* energy levels of the quadruplex formation are: $\Delta H_{\text{base}} \sim -7 \text{ kcal mol}^{-1}$ and $\Delta S_{\text{base}} \sim -20 \text{ cal mol}^{-1} \text{ K}^{-1}$ for i-motifs⁸ as compared to $\Delta H_{\text{base}} \sim -5 \text{ kcal mol}^{-1}$ and $\Delta S_{\text{base}} \sim -12 \text{ cal mol}^{-1} \text{ K}^{-1}$ for a regular Watson-Crick G/C base pair.⁹

The folding/unfolding kinetics of the i-motif based systems shows similar timescales to many crucial processes in living systems involving changes in pH (within the scale of seconds to hours).¹⁰ For example, folding/unfolding times of about 100 ms were demonstrated for unmodified i-motifs.¹¹ This timescale is slower than the timescale for an alternative highly responsive system (based on micellar nanoparticles, with response times on the scale of 4 ms, as discussed in the main text)¹² but compatible with the majority of the processes in living systems. For example, i-motif-based sensors (with adequate temporal resolution) provide adequate response rate for monitoring changes associated with endosome maturation,¹³ mapping pH along intersecting endocytic pathways,¹⁴ and/or mapping pH changes in *C. elegans*.¹⁵

It has been established that cytidines can form a hemiprotonated base pairs in acidic conditions (ref.³ and references therein, and Scheme S1). Furthermore, single-stranded oligonucleotides containing at least 4 tracts of cytosines can fold into an intramolecular tetraplex structure called an i-motif.^{1,4} The tetraplexes are mediated by the hemiprotonated Cytidine-H⁺-Cytidine base pairs (Figure 2 in the main text or more detailed in Scheme S1). The stability of the tetraplexes is pH-dependent.¹ In general, at pH above 4.5, the stability of the i-motifs decreases with increasing pH.¹ The length of cytosine tracts has a strong impact on stability of the i-motifs: for the cytosine stretches ranging between 2 and 5, the addition of each Cytidine-H⁺-Cytidine base pair results in ΔG_{37} (Gibbs free energy of formation at 37 °C) decrease of about 3 kcal mol⁻¹. In addition, an i-motif stability depends on the nature of loops between C-tracts^{1,5} (i-loops in Figure 2 in the main text). The nature of the effect has not been well understood and thus needs to be carefully investigated. Among potential reasons for the i-loop-dependent stabilization/destabilization of an i-motif could be formation of transient base pairs in loops (e.g. between As and Ts in loops of AAT or TTA

Table S1. Sequences of oligonucleotides used throughout the study. Fragments composing hairpin stems are italicized, loops – underlined. **RG** = Rhodamine Green.

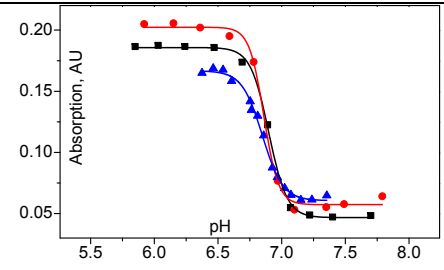
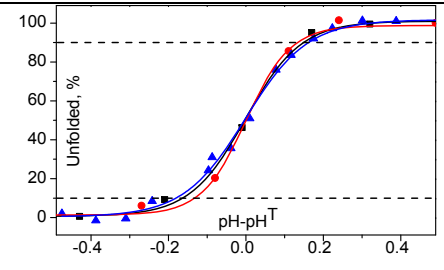
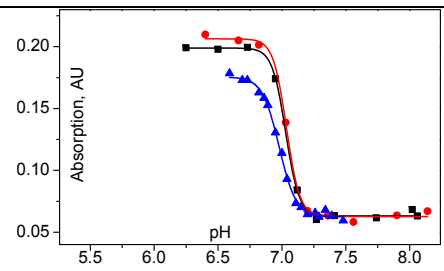
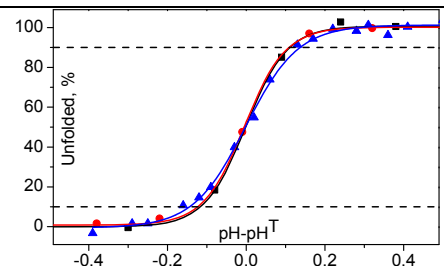
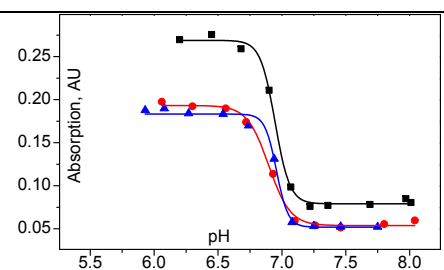
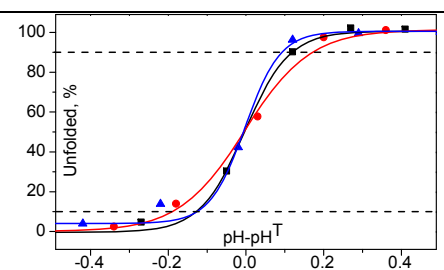
Name (as mentioned in the text)	Sequence, 5'→3'
(C ₅ T ₃) ₃ C ₅	CCC CCT TTC CCC CTT TCC CCC TTT CCC CC
(C ₄ A ₃) ₃ C ₄	CCC CAA ACC CCA AAC CCC AAA CCC C
(C ₄ AAT) ₃ C ₄	CCC CAA TCC CCA ATC CCC AAT CCC C
(C ₄ TTA) ₃ C ₄	CCC CTT ACC CCT TAC CCC TTA CCC C
(C ₅ AAT) ₃ C ₅	CCC CCA ATC CCC CAA TCC CCC AAT CCC CC
(C ₅ TTA) ₃ C ₅	CCC CCT TAC CCC CTT ACC CCC TTA CCC CC
(C ₄ T ₃) ₃ C ₄	CCC CTT TCC CCT TTC CCC TTT CCC C
(C ₄ T ₄) ₃ C ₄	CCC CTT TTC CCC TTT TCC CCT TTT CCC C
(C ₅ T ₄) ₃ C ₅	CCC CCT TTT CCC CCT TTT CCC CCT TTT CCC CC
(C ₅ T ₃) ₃ C ₅ + EH: stem 7, loop 14	<i>CTT CTT <u>CAA TAC TAC</u> CCC CTT TCC CCC TTT CCC CCT TTC CCC CCT <u>CTC TAG AAG AAG</u></i>
(C ₅ T ₃) ₃ C ₅ + EH: stem 7, loop 7	<i>CTT CTT <u>CAA TCC</u> CCC TTT CCC CCT TTC CCC CTT TCC CCC <u>ACT CGA AGA AG</u></i>
(C ₅ T ₃) ₃ C ₅ + EH: stem 7, loop 0	<i>CTT CTT CCC CCC TTT CCC CCT TTC CCC CTT TCC CCC <u>GAA GAA G</u></i>
(C ₄ TTA) ₃ C ₄ + EH	<i>CTA TAT <u>AAA</u> CCC CTT ACC CCT TAC CCC TTA CCC <u>CCT CTA TAT AG</u></i>
(C ₅ T ₄) ₃ C ₅ + IH	CCC CCT TTT CCC CCA <i>CTT ATT <u>AAA CTC TAA TAA GAC</u> CCC CTT TTC CCC C</i>
(C ₅ T ₃) ₃ C ₅ ^{FL}	RG-CCC CCT TTC CCC CTT TCC CCC TTT CCC CC-Dabcyl
(C ₄ TTA) ₃ C ₄ + EH ^{FL}	RG-CTA TAT <u>AAA</u> CCC CTT ACC CCT TAC CCC TTA CCC <u>CCT CTA TAT AG-Dabcyl</u>
(C ₅ T ₄) ₃ C ₅ + IH ^{FL}	RG-CCC CCT TTT CCC CCA <i>CTT ATT <u>AAA CTC TAA TAA GAC</u> CCC CTT TTC CCC C-Dabcyl</i>

Table S2. Summary of pH denaturation data. The graphs in columns titled “pH denaturation profiles” and “Transition widths: replicates” have been used to calculate average values and standard deviations for the results in columns “ pH^T ”, “ ΔpH_{10-90} ”, and “ n ”.

Sequence	pH denaturation profiles: replicates	pH^T	Transition widths: replicates ^a	ΔpH_{10-90} ^a	n ^a
(C ₄ AAT) ₃ C ₄		6.54 ± 0.03		0.29 ± 0.02	6.6 ± 0.2
(C ₄ A ₃) ₃ C ₄		6.45 ± 0.03		0.33 ± 0.04	6.2 ± 0.8
(C ₄ T ₃) ₃ C ₄		6.77 ± 0.01		0.33 ± 0.03	6.2 ± 0.6

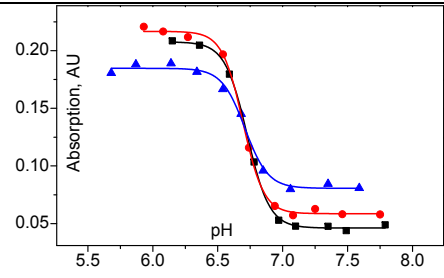
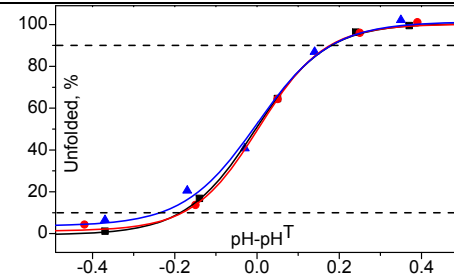
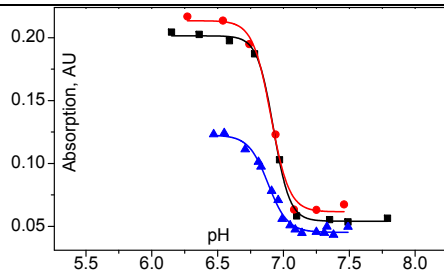
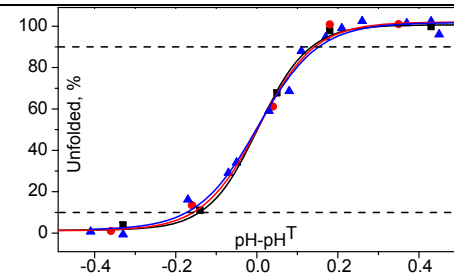
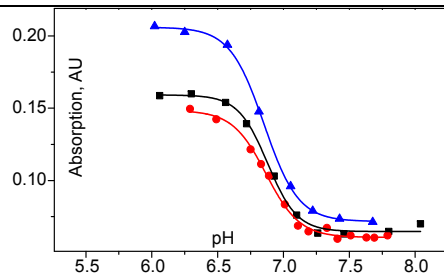
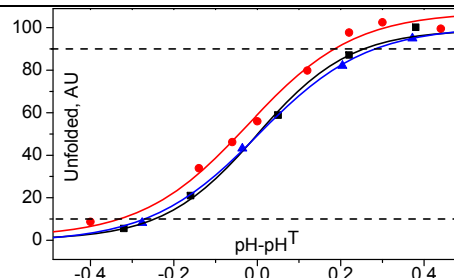
The Table S2 is continued on the next page.

Table S2. Continued from the previous page.

Sequence	pH denaturation profiles: replicates	pH^T	Transition widths: replicates ^a	ΔpH_{10-90}^a	n^a
$(C_4T_4)_3C_4$		6.88 ± 0.03		0.31 ± 0.04	6.4 ± 1.0
$(C_5T_4)_3C_5$		7.02 ± 0.03		0.25 ± 0.03	7.6 ± 1.0
$(C_5T_3)_3C_5$		6.94 ± 0.02		0.28 ± 0.08	7.2 ± 2.1

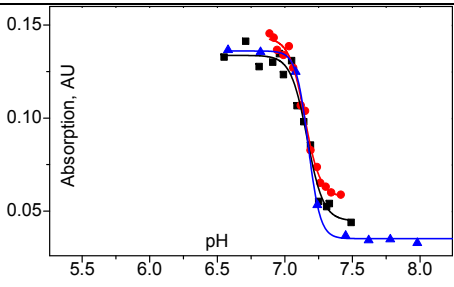
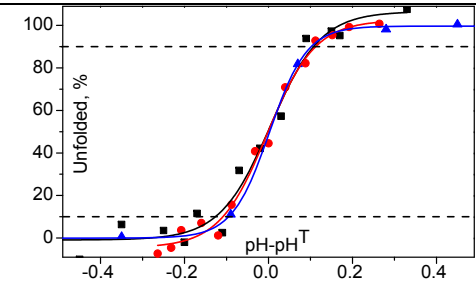
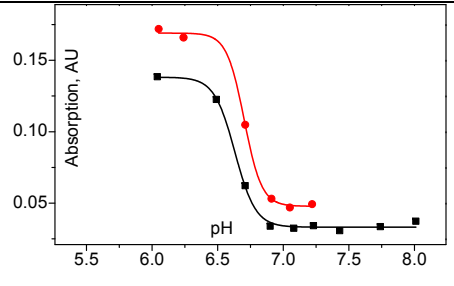
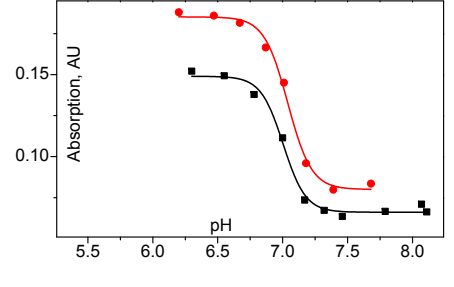
The Table S2 is continued on the next page.

Table S2. Continued from the previous page.

Sequence	pH denaturation profiles: replicates	pH^T	Transition widths: replicates ^a	ΔpH_{10-90}^a	n^a
$(C_4TTA)_3C_4$		6.71 ± 0.02		0.39 ± 0.03	5.3 ± 0.3
$(C_5TTA)_3C_5$		6.90 ± 0.02		0.30 ± 0.02	6.5 ± 0.6
$(C_4TTA)_3C_4+EH$		6.87 ± 0.02		0.53 ± 0.02	4.2 ± 0.3

The Table S2 is continued on the next page.

Table S2. Continued from the previous page.

Sequence	pH denaturation profiles: replicates	pH^T	Transition widths: replicates ^a	ΔpH_{10-90} ^a	n^a
$(C_5T_4)_3C_4+IH$		7.16 ± 0.01		0.22 ± 0.01	7.8 ± 1.3
$(C_5AAT)_3C_5$		6.63 ± 0.05	ND	ND	ND
$(C_5T_3)_3C_5+EH$ S7/L14		7.00 ± 0.03	ND	ND	ND

^a “ND” = not determined

The Table S2 is continued on the next page.

Table S2. Continued from the previous page.

Sequence	pH denaturation profiles: replicates	pH^T	Transition widths: replicates ^a	ΔpH_{10-90} ^a	n^a
(C ₅ T ₃) ₃ C ₅ +EH S7/L7		7.13 ± 0.02	ND	ND	ND
(C ₅ T ₃) ₃ C ₅ +EH S7/L0		7.22 ± 0.04	ND	ND	ND

^a "ND" = not determined

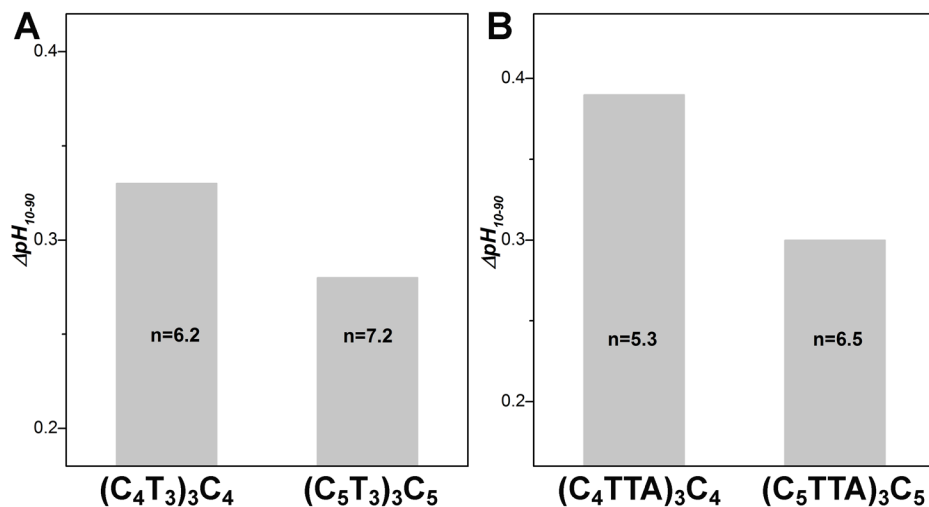
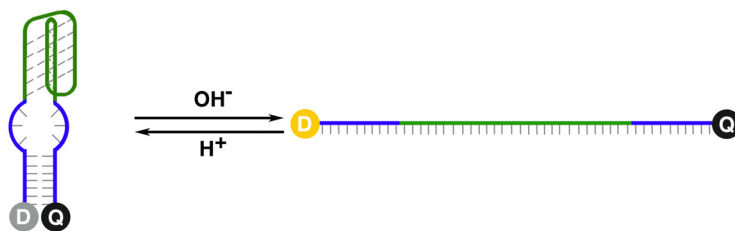


Figure S1. Effect of an i-motif C-tract length on its folding cooperativity (in terms of Hill coefficient, n) and on transition width (in terms of ΔpH_{10-90} , Y axis) for 4- and 5-cytidine C-tracts with TTT (plane A) and TTA (plane B) i-loops. The results were derived from pH-triggered denaturations monitored via UV absorption at 295 nm. All the sequences are included in Table S1.

Scheme of sensor (C₅T₃)₃C₅^{FL}:



Scheme of sensor (C₄TTA)₃C₄+EH^{FL}:



Scheme of sensor (C₅T₄)₃C₅+IH^{FL}:

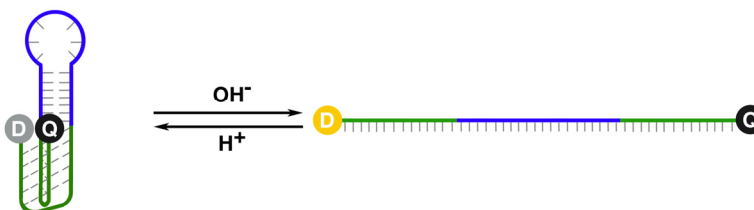


Figure S2. Schemes of fluorescent sensors.

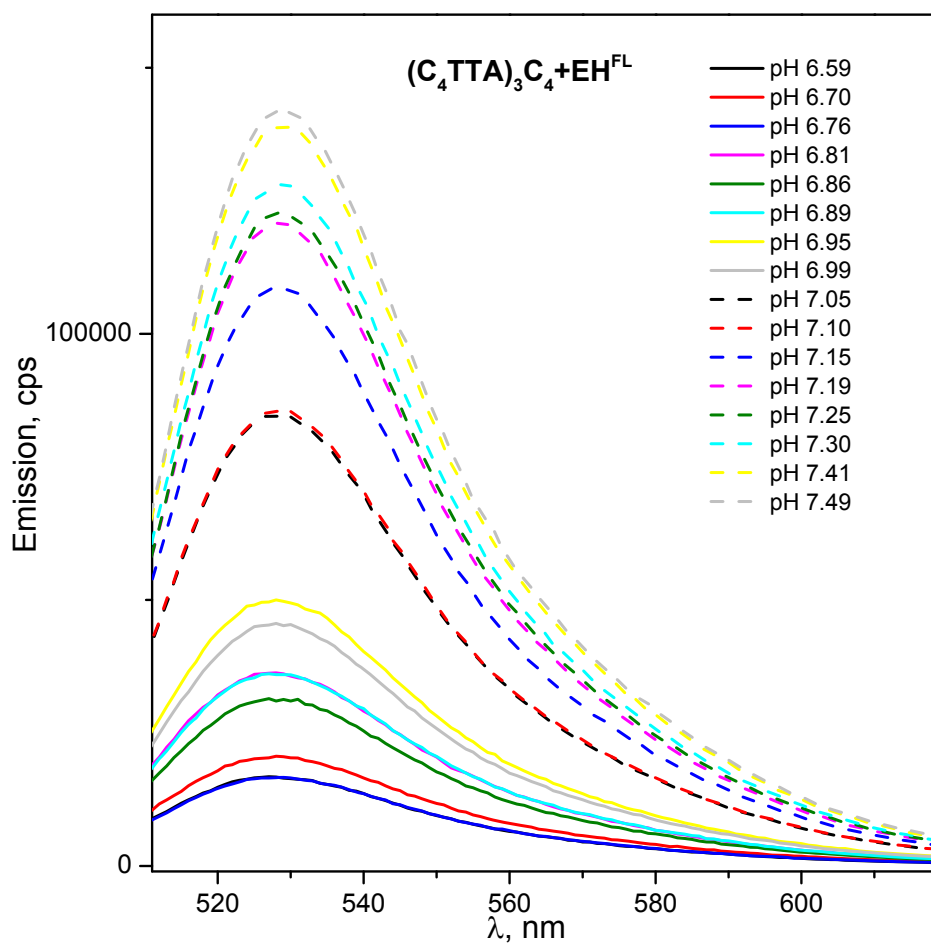


Figure S3. Emission of sensor $(C_4TTA)_3C_4+EH^{FL}$ at different pH values. The sensor was labeled with the Rhodamine Green/Dabcyl donor/quencher pair. Emission of Rhodamine Green was recorded from 510 to 650 nm with the excitation wavelength of 495 nm. The sensor concentration was approx. 100 nM in Na_2HPO_4 (20 mM)/KCl (100 mM) buffer solutions.

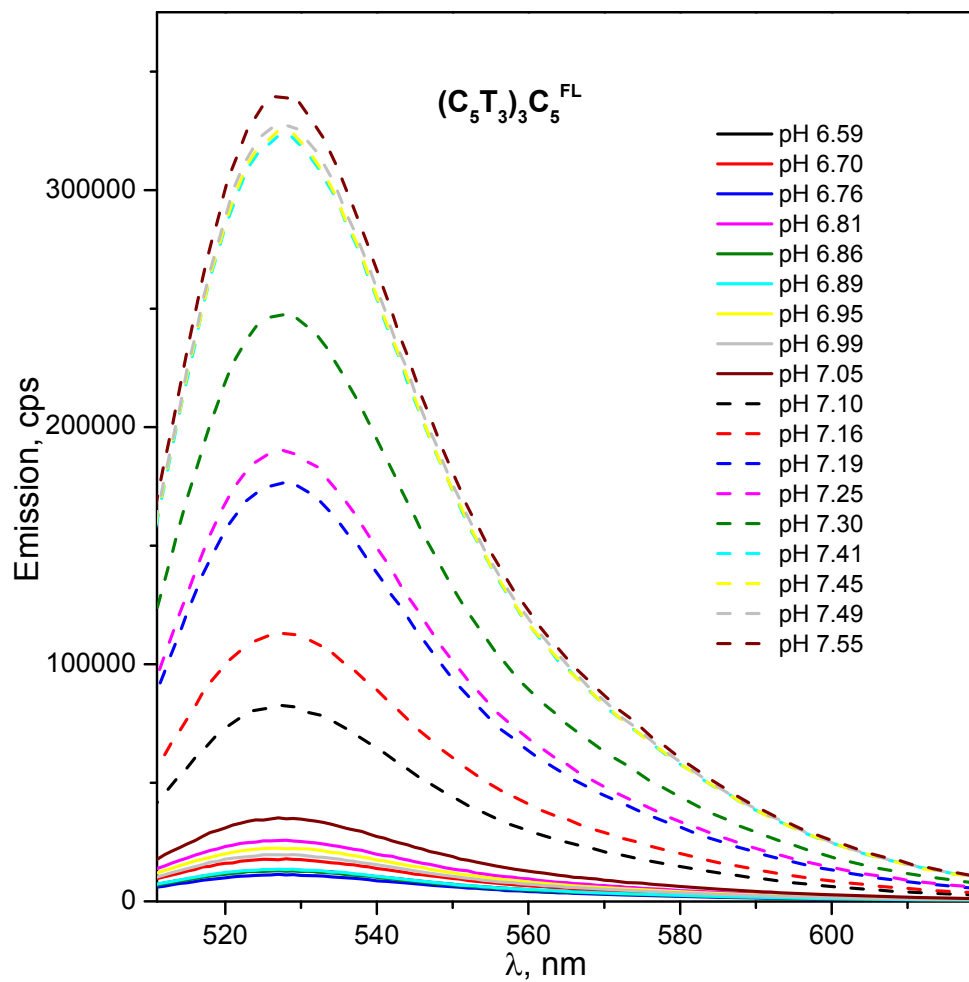


Figure S4. Emission of sensor $(C_5T_3)_3C_5^{FL}$ at different pH values. The sensor was labeled with the Rhodamine Green/Dabcyl donor/quencher pair. Emission of Rhodamine Green was recorded from 510 to 650 nm with the excitation wavelength of 495 nm. The sensor concentration was approx. 100 nM in Na_2HPO_4 (20 mM)/KCl (100 mM) buffer solutions.

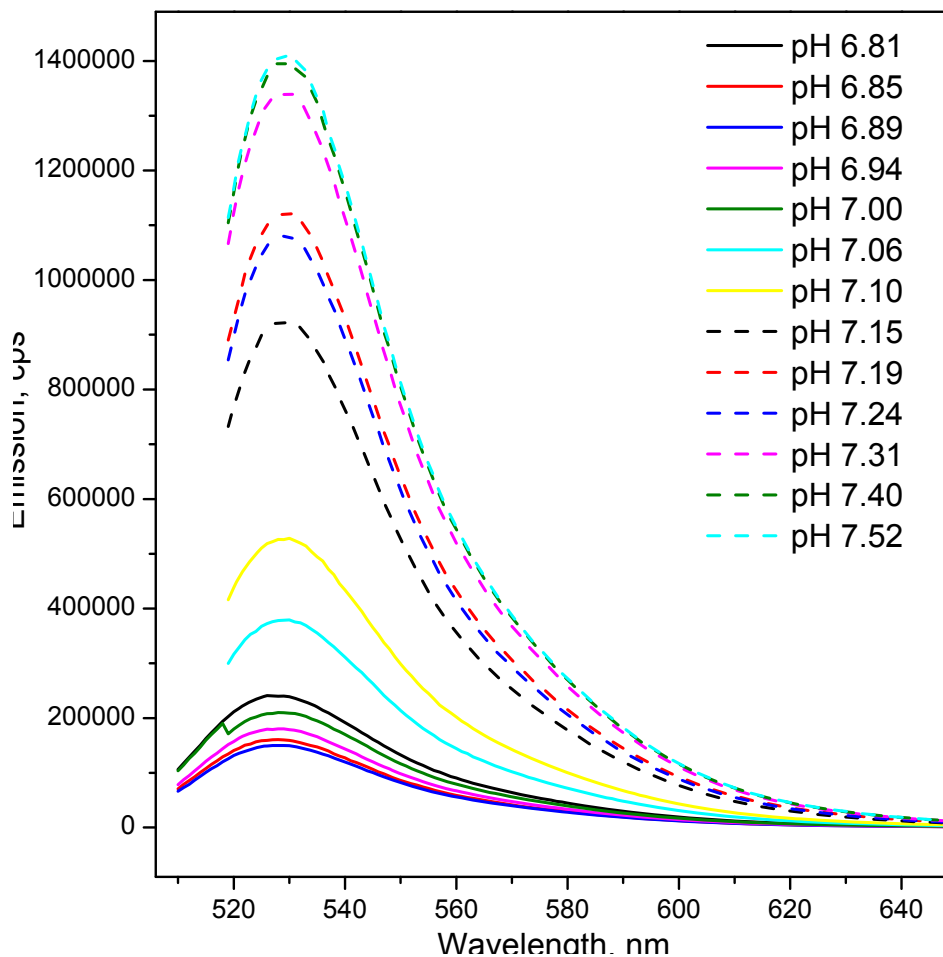


Figure S5. Emission of sensor $(C_5T_4)_3C_5+IH^{FL}$ at different pH values. The sensor was labeled with the Rhodamine Green/Dabcyl donor/quencher pair. Emission of Rhodamine Green was recorded from 510 to 650 nm with the excitation wavelength of 495 nm. The sensor concentration was approx. 100 nM in Na_2HPO_4 (20 mM)/KCl (100 mM) buffer solutions.

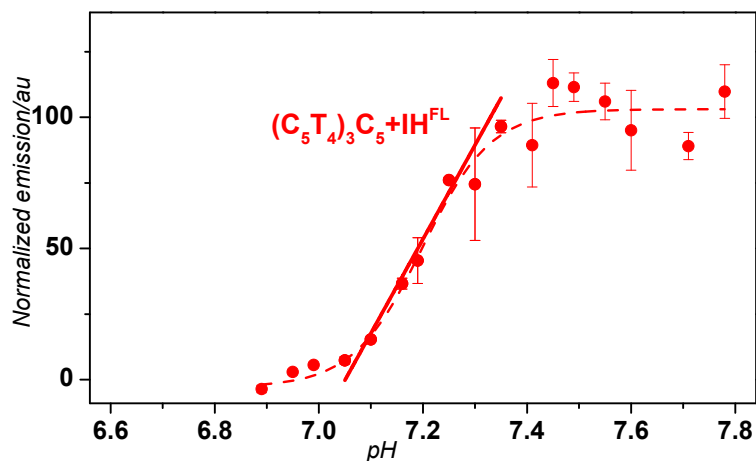


Figure S6. Fluorescent response of sensor $(C_5T_4)_3C_5+IH^{FL}$ on pH changes. The sensor was labeled with the Rhodamine Green/Dabcyl donor/quencher pair. Emission of Rhodamine Green was recorded from 510 to 650 nm with the excitation wavelength of 495 nm. The sensor concentration was approx. 100 nM in Na_2HPO_4 (20 mM)/KCl (100 mM) buffer solutions. The experiment on this graph is a repeat of corresponding experiment presented in Figure 5 in the main text. The characteristics for this curve are: $\Delta pH_{10-90} = 0.23$; linear range 0.30 pH units

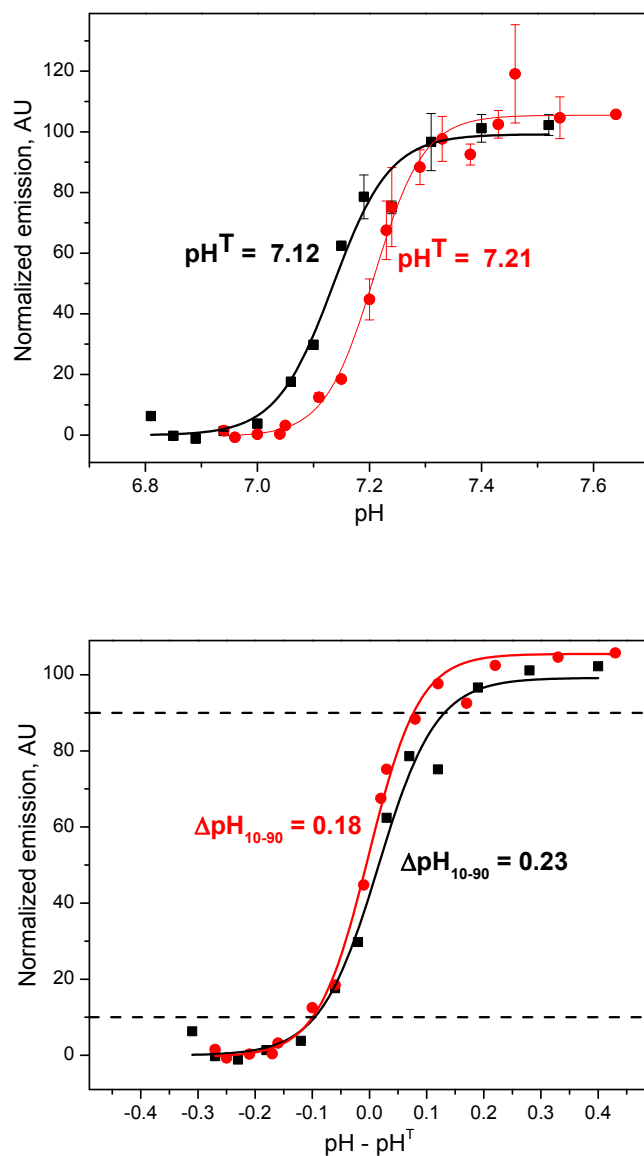


Figure S7. Profile of pH-triggered transition of sensor $((\text{C}_5\text{T}_4)_3\text{C}_5 + \text{IH}^{\text{FL}}$ in Na_2HPO_4 (20 mM)/KCl (100mM) buffer (black traces) and in the presence of 20 % FBS (red traces). The raw experimental data are presented in Figure S8. The lower panel illustrates differences in response width. Dotted horizontal lines indicate 10 % and 90 % signal values.

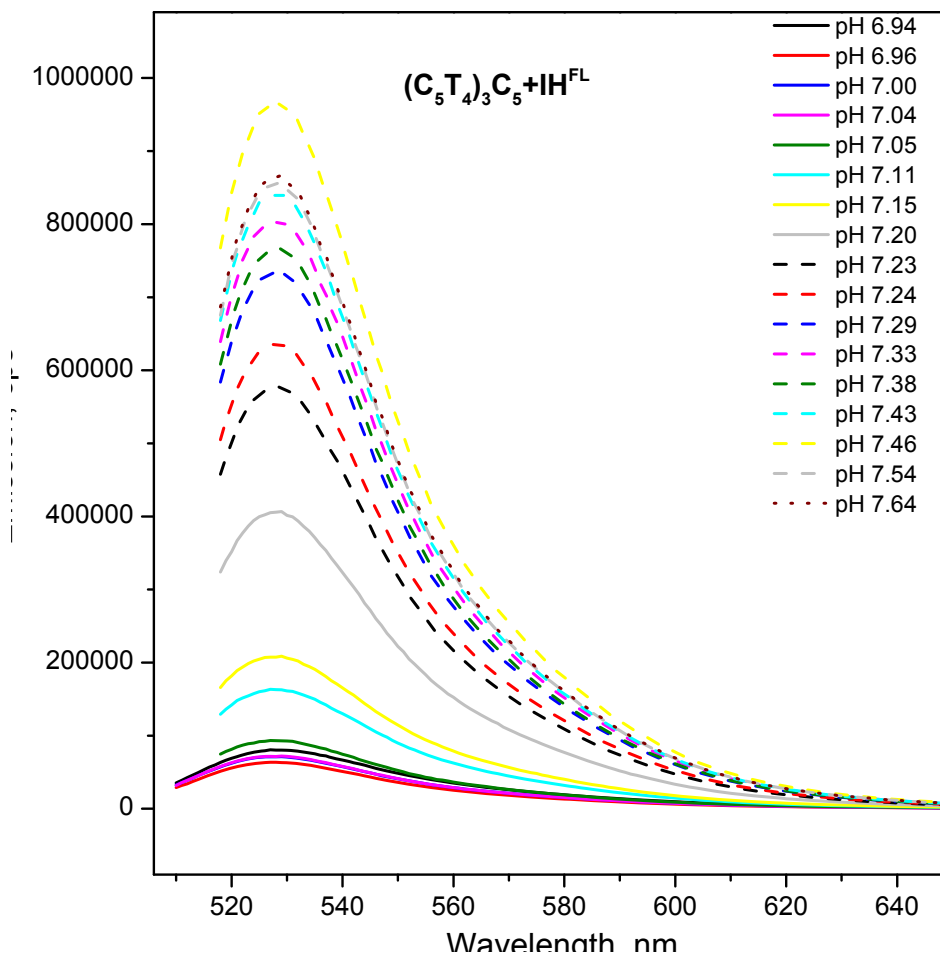


Figure S8 Emission of sensor $(C_5T_4)_3C_5+IH^{FL}$ at different pH values in phosphate buffer in the presence of 20 % FBS. The sensor was labeled with Rhodamine Green/Dabcyl donor/quencher pair. Emission of Rhodamine Green was recorded between 515 to 650 nm with the excitation wavelength of 495 nm. The sensor concentration was approx. 100 nM.

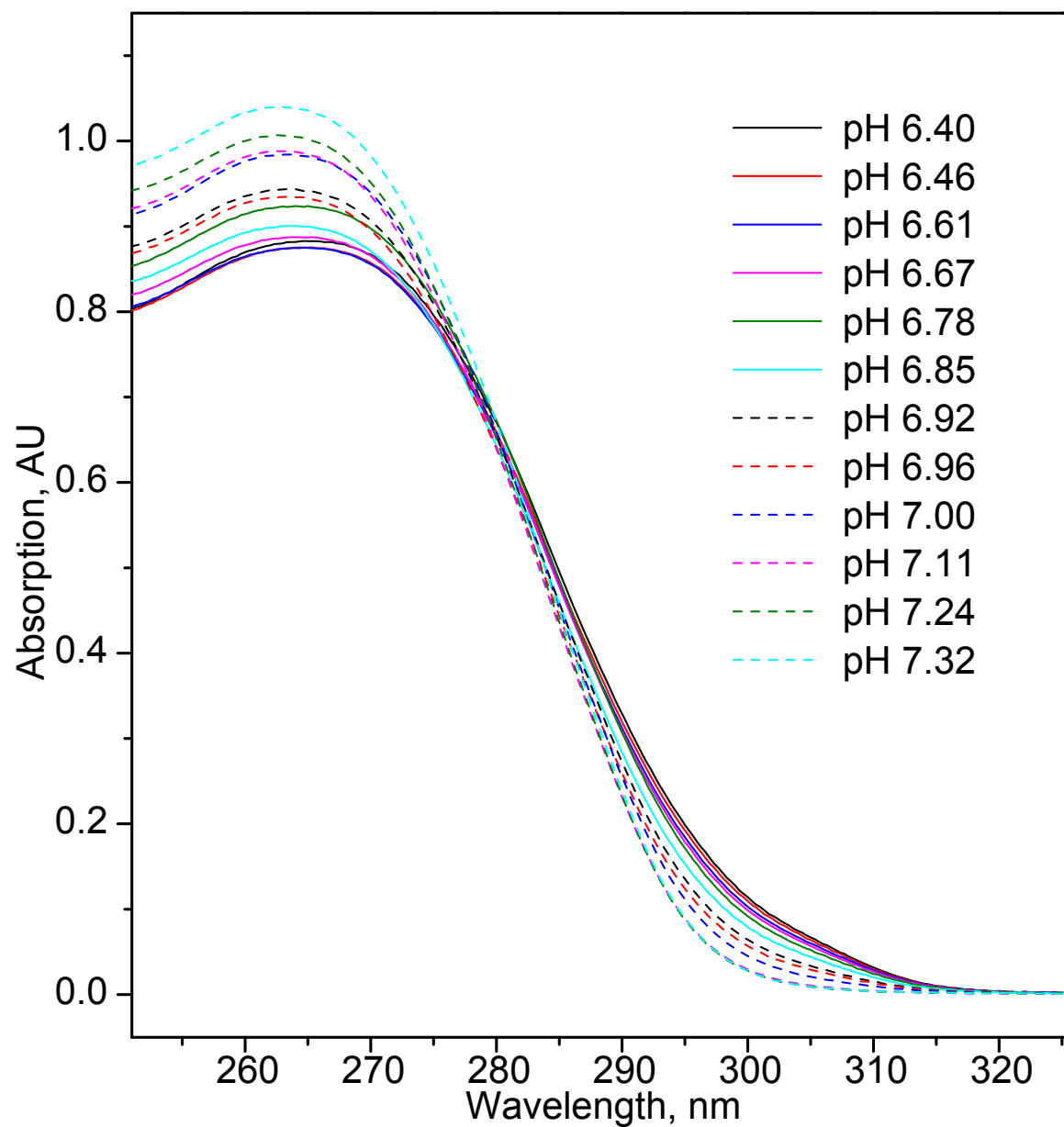


Figure S9. UV absorption spectra of oligonucleotide $(C_4TTA)_3C_4$ + EH at various pH values. Oligonucleotide concentration was $\sim 3 \mu\text{M}$.

References (for Supporting Information)

- (1) Mergny, J. L.; Lacroix, L.; Han, X. G.; Leroy, J. L.; Hélène, C. *J. Am. Chem. Soc.* **1995**, *117*, 8887-8898.
- (2) Mergny, J.-L.; Lacroix, L. *Nucleic Acids Res.* **1998**, *26*, 4797-4803.
- (3) Gehring, K.; Leroy, J.-L.; Guéron, M. *Nature* **1993**, *363*, 561-565.
- (4) (a) Ahmed, S.; Kintanar, A.; Henderson, E. *Nat. Struct. Biol.* **1994**, *1*, 83-88; (b) Ahmed, S.; Henderson, E. *Nucleic Acids Res.* **1992**, *20*, 507-511; (c) Leroy, J. L.; Guéron, M.; Mergny, J. L.; Hélène, C. *Nucleic Acids Res.* **1994**, *22*, 1600-1606.
- (5) (a) Nonin, S.; Phan, A. T.; Leroy, J.-L. *Structure* **1997**, *5*, 1231-1246; (b) Yang, Y.; Sun, Y.; Yang, Y.; Xing, Y.; Zhang, T.; Wang, Z.; Yang, Z.; Liu, D. *Macromolecules* **2012**, *45*, 2643-2647.
- (6) (a) Chakraborty, S.; Sharma, S.; Maiti, P. K.; Krishnan, Y. *Nucleic Acids Res.* **2009**, *37*, 2810-2817; (b) Saha, S.; Bhatia, D.; Krishnan, Y. *Small* **2010**, *6*, 1288-1292; (c) Saha, S.; Chakraborty, K.; Krishnan, Y. *Chem. Commun.* **2012**, *48*, 2513-2515.
- (7) (a) Goddard, N. L.; Bonnet, G.; Krichevsky, O.; Libchaber, A. *Phys. Rev. Lett.* **2000**, *85*, 2400-2403; (b) Wallace, M. I.; Ying, L.; Balasubramanian, S.; Klenerman, D. *Proc. Natl. Acad. Sci. U.S.A.* **2001**, *98*, 5584-5589.
- (8) Völker, J.; Klump, H. H.; Breslauer, K. J. *Biopolymers* **2007**, *86*, 136-147.
- (9) SantaLucia, J.; Hicks, D. *Annu. Rev. Biophys. Biomolec. Struct.* **2004**, *33*, 415-440.
- (10) (a) Lin, H.-J.; Herman, P.; Lakowicz, J. R. *Cytometry, Part A* **2003**, *52A*, 77-89; (b) Jensen, M. S.; Bainton, D. F. *J. Cell Biol.* **1973**, *56*, 379-388; (c) Geisow, M. J.; Hart, P. D.; Young, M. R. *J. Cell Biol.* **1981**, *89*, 645-652.
- (11) Chen, C.; Li, M.; Xing, Y.; Li, Y.; Joedecke, C.-C.; Jin, J.; Yang, Z.; Liu, D. *Langmuir* **2012**, *28*, 17743-17748.
- (12) Zhou, K.; Wang, Y.; Huang, X.; Luby-Phelps, K.; Sumer, B. D.; Gao, J. *Angew. Chem., Int. Ed.* **2011**, *50*, 6109-6114.
- (13) Modi, S.; Swetha, M. G.; Goswami, D.; Gupta, G. D.; Mayor, S.; Krishnan, Y. *Nat. Nanotechnol.* **2009**, *4*, 325-330.
- (14) Modi, S.; Nizak, C.; Surana, S.; Halder, S.; Krishnan, Y. *Nat. Nanotechnol.* **2013**, *8*, 459-467.
- (15) Surana, S.; Bhat, J. M.; Koushika, S. P.; Krishnan, Y. *Nat. Commun.* **2011**, *2*, 1-7.